

**Cell Reports, Volume 31**

**Supplemental Information**

**Kainate Receptor Activation Shapes Short-Term**

**Synaptic Plasticity by Controlling Receptor**

**Lateral Mobility at Glutamatergic Synapses**

**Alice Polenghi, Thierry Nieu, Stefania Guazzi, Pau Gorostiza, Enrica Maria Petrini, and Andrea Barberis**

## Supplementary information

**Figure S1**

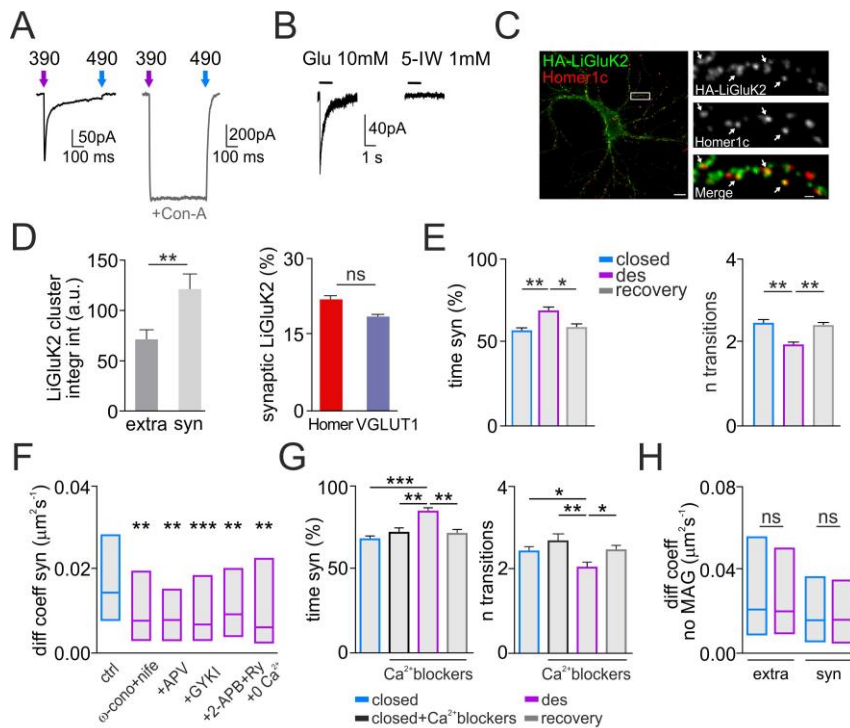


**Figure S1. Functional and diffusion properties of LiGluK2 receptors (Related to Figure 1)**

**(A)** Left panel: Representative traces of activation and deactivation of LiGluK2 receptor-mediated currents induced by illumination with 380 nm and 488 nm light, respectively. Note that the current onset is followed by fast and profound desensitization. Right panel: Representative traces of activation and deactivation of LiGluK2 receptor-mediated currents induced by illumination at 380 nm and 488 nm, respectively in the presence of Concanavalin-A (Con-A, 0.1 mg/ml). Note that Con-A abolishes the LiGluK2 desensitization thus preventing the fading of the current and induces a ~5-fold current amplitude increase. **(B)** Left Panel: Application of 10 mM glutamate puffs in the presence of GYKY 53655 and D-APV leads to activation and desensitization of LiGluK2. Right panel: Application of 5-IW (1 mM) does not elicit sizable current, suggesting the absence of GluK5 subunit. **(C)** Left panel: Representative image of surface HA-LiGluK2 immunoreactivity in a cultured hippocampal neuron (green) co-transfected with Homer1c-DsRed (red). Scale bar, 10  $\mu$ M. Right panel: Detail of the dendrite portion framed on the left panel, showing HA-LiGluK2 clusters (top), Homer1c clusters (middle) and LiGluK2-Homer1c clusters colocalization (bottom, arrows). Scale bar, 1  $\mu$ M. **(D)** Left panel: Quantification of immunocytochemistry experiments of LiGluK2 synaptic clusters. Note that the integrated fluorescence intensity of synaptic LiGluK2 clusters is significantly increased with

respect to the non-synaptic areas. Right panel: Percentage of synaptic LiGluK2 defined as those colocalizing with the postsynaptic marker Homer1c or juxtaposed to the presynaptic marker VGLUT1 (n= 48 cells for each condition from 3 independent cultures). **(E)** Percentage of time spent at the synapse (left panel) and number of transitions (right panel) of LiGluK2 at synapses. In the desensitized state, LiGluK2 spent more time at synapses and displayed lower number of transitions between extrasynaptic and synaptic compartments ( $n_{\text{trajectories closed}}= 255$ ,  $n_{\text{trajectories des}}= 186$ ,  $n_{\text{trajectories recovery}}= 245$ , from 3 independent cultures, Mann-Whitney test). **(F)** Summary of median diffusion coefficient and IQR of synaptic LiGluK2 in the closed (blue) and desensitized state (purple) when nifedipine/ $\Omega$ -conotoxin MVIIC, D-APV, GYKI 53655 and 2-APB/ryanodine are sequentially bath applied to block voltage gated calcium channels (VGCC), NMDA receptors (NMDAR), AMPA receptors (AMPA) and IP3/ryanodine receptors, respectively. **(G)** Summary of percentage of time spent by LiGluK2 at synaptic compartment (left panel) and LiGluK2 number of synaptic transitions (right panel) in the closed state (blue,  $n_{\text{trajectories}}= 255$ ), closed state in the presence of the VGCC blockers cocktail (black,  $n_{\text{trajectories}}= 105$ ), desensitized state in the presence of the VGCC blockers cocktail (purple,  $n_{\text{trajectories}}= 100$ ) and in the recovery state (grey,  $n_{\text{trajectories}}= 118$ , Student's test). For the detailed experimental protocol see Figure 1E. **(H)** Summary of median diffusion coefficient and IQR of extrasynaptic ( $n_{\text{trajectories}}=136$ ; ns, Mann-Whitney U-test) and synaptic LiGluK2 ( $n_{\text{trajectories}}=100$ ; ns, Mann-Whitney U-test) without MAG labeling. In the absence of MAG, the LiGluK2 diffusion properties during illumination at 380 nm (purple) are indistinguishable from the control (blue). Unless otherwise stated data are presented as mean  $\pm$  SEM, \*P < 0.05; \*\*P < 0.01; \*\*\*P < 0.001 and ns, non-significant.

**Figure S2**

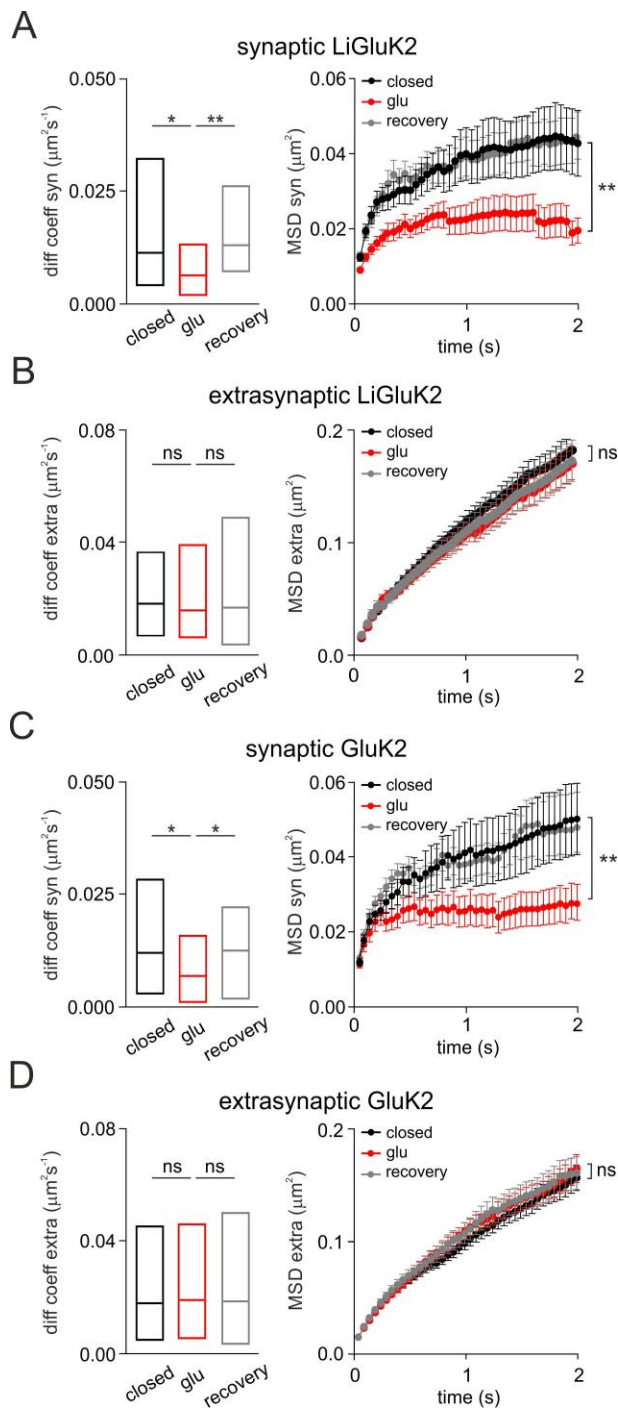


**Figure S2. Diffusion properties of synaptic and extrasynaptic LiGluK2 and GluK2 receptors in control condition and in the presence of glutamate (Related to Figure 1)**

**(A)** Summary of diffusion coefficient (left panel) and MSD vs time curves (right panel) of synaptic LiGluK2 in control (black,  $n_{\text{trajectories}} = 61$ ), during application of  $100 \mu\text{M}$  glutamate (red,  $n_{\text{trajectories}} = 50$ )

and after glutamate wash out (grey,  $n_{\text{trajectories}}= 43$ ). Note that values of diffusion coefficient of synaptic LiGluK2 receptors in the different conditions are undistinguishable with respect to that obtained with the GluK2 receptors. Receptor lateral diffusion was monitored in the continued presence of VGCC blockers and in nominal zero  $\text{Ca}^{2+}$  solution (see Fig.1). **(B)** Summary of median diffusion coefficient and IQR (left panel panel) and MSD vs time curves (right panel) of extrasynaptic LiGluK2 in control (black,  $n_{\text{trajectories}} = 179$ ), during application of 100  $\mu\text{M}$  glutamate (red,  $n_{\text{trajectories}} = 158$ ) and after glutamate wash out (grey,  $n_{\text{trajectories}}= 142$ , ns, Mann–Whitney U-test). **(C)** Summary of median diffusion coefficient and IQR (left panel panel) and MSD vs time curves (right panel) of synaptic GluK2 in control (black,  $n_{\text{trajectories}} = 64$ ), during application of 100  $\mu\text{M}$  glutamate (red,  $n_{\text{trajectories}} = 70$ ) and after glutamate wash out (grey,  $n_{\text{trajectories}}= 34$ ), from 4 neurons from 2 independent cultures. Note that bath application of glutamate induced the immobilization of synaptic GluK2 receptors (red). Receptor lateral diffusion was monitored in the continued presence of VGCC blockers (see Fig.1). **(D)** Summary of median diffusion coefficient and IQR (left panel panel) and MSD vs time curves (right panel) of extrasynaptic GluK2 in control (black,  $n_{\text{trajectories}} = 204$ ), during application of 100  $\mu\text{M}$  glutamate (red,  $n_{\text{trajectories}} = 196$ ) and after glutamate wash out (grey,  $n_{\text{trajectories}}= 175$ , ns, Mann–Whitney U-test). Note that the application of glutamate does not change the diffusion properties of extrasynaptic GluK2 receptors. Unless otherwise stated, data are presented as mean  $\pm$  SEM, \* $P<0.05$ ; \*\* $P<0.01$ ; \*\*\* $P<0.005$ ; ns: non-significant.

Figure S3

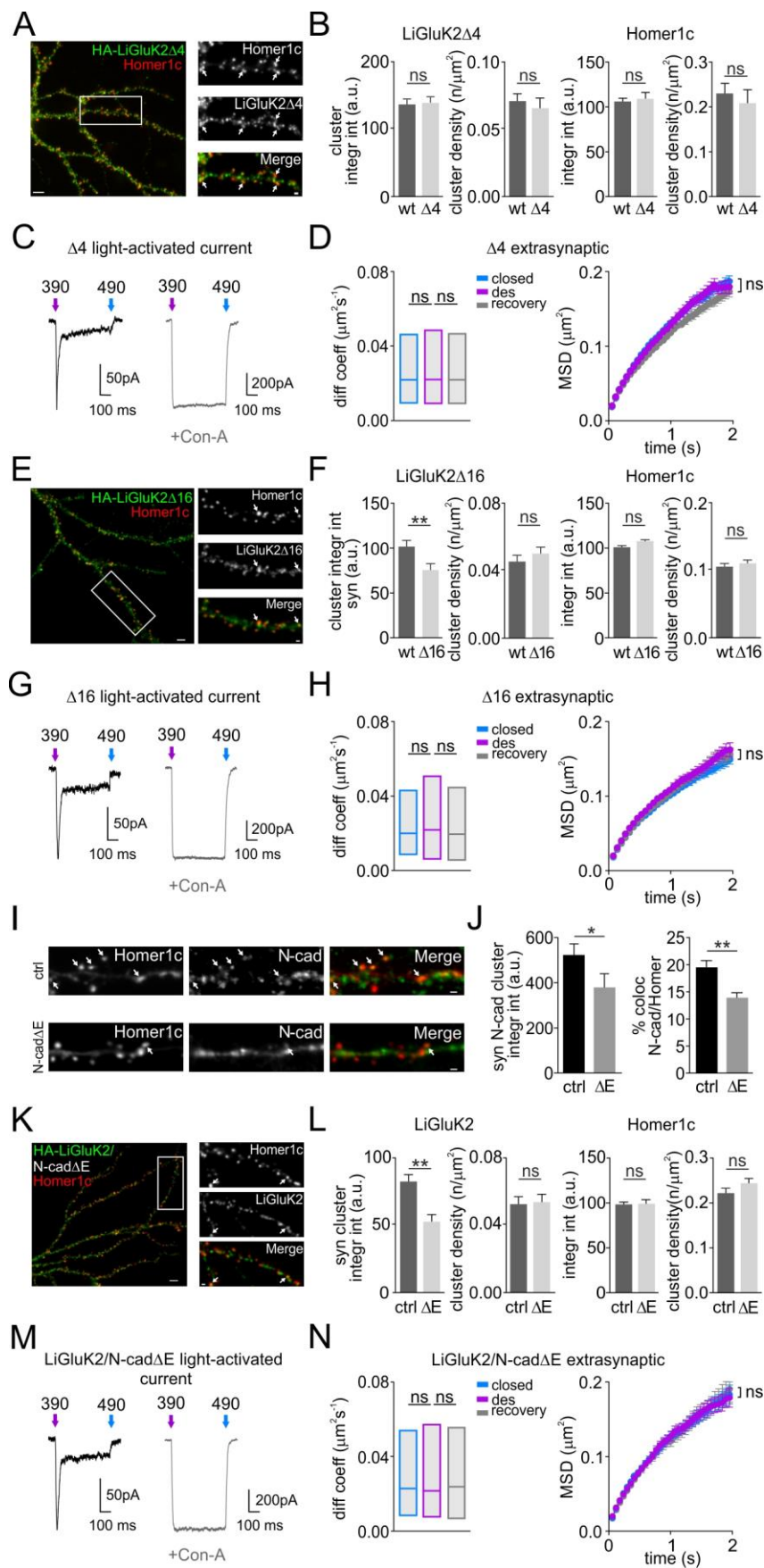


**Figure S3. Surface expression, functional properties and diffusive properties of LiGluK2 $\Delta$ 4, LiGluK2 $\Delta$ 16 and LiGluK2/N-cad $\Delta$ E receptors (Related to Figure 2)**

**(A)** Left panel: Representative multicolor fluorescence image of the distribution of surface HA-LiGluK2 $\Delta$ 4 receptors (green) and their colocalization with the postsynaptic marker Homer1c (red) in cultured hippocampal neurons. Scale bar, 10  $\mu$ M. Right panel: Magnification of the portion of a dendrite framed on the left panel, showing HA-LiGluK2 clusters (top), Homer1c clusters (middle,) and the LiGluK2-Homer1c colocalization (bottom). Arrows indicate synaptic clusters. Scale bar, 1  $\mu$ M.

**(B)** Left panel. Quantification of synaptic integrated fluorescence intensity and density of LiGluK2 (wt) and LiGluK2 $\Delta$ 4 ( $\Delta$ 4) clusters (n=19 and n=22, respectively, from 2 independent cultures,  $P > 0.05$ , Student's t-test). Right panel. Quantification of integrated fluorescence and density of Homer1c clusters in LiGluK2 and LiGluK2 $\Delta$ 4 expressing neurons. Note that the deletion of the PDZ binding domain does not affect the expression and the distribution of Homer1c puncta.

**(C)** Representative averaged traces of light-evoked LiGluK2 $\Delta$ 4 receptor-mediated currents in the absence (left panel) or presence (right panel) of Concanavalin-A (0.1 mg/ml). LiGluK2 $\Delta$ 4 activations and deactivations were elicited by illuminations with 380 nm and 488 nm light, respectively. The LiGluK2 $\Delta$ 4-mediated current onset is followed by fast and profound desensitization. This desensitization is abolished when Con-A is added, thus inducing a  $\sim$  5-fold current amplitude increase, similarly to LiGluK2-mediated currents (compare with Supplementary Figure 1A).

**(D)** Summary of median diffusion coefficient and IQR (left panel) and MSD vs time curve (right panel) of extrasynaptic LiGluK2 $\Delta$ 4 in the closed state ( $n_{\text{trajectories}} = 558$ , blue), desensitized state ( $n_{\text{trajectories}} = 448$ , purple) and closed recovery state ( $n_{\text{trajectories}} = 521$ , grey, from 8 neurons, ns, Mann-Whitney U-test).

**(E)** Left panel. Distribution and colocalization of LiGluK2 $\Delta$ 16 (green) with the postsynaptic marker Homer1c (red) in cultured hippocampal neurons. Scale bar, 10  $\mu$ M. Right panel: Detail of the dendrite framed portion showing LiGluK2 $\Delta$ 16 clusters (top), Homer1c clusters (middle) and the LiGluK2-Homer1c colocalization (bottom, arrows). Scale bar, 1  $\mu$ M.

**(F)** Left panel. Summary of immunocytochemistry experiments showing the integrated intensity of HA-LiGluK2 $\Delta$ 16 and the HA-LiGluK2 $\Delta$ 16 dendritic cluster density (n=36 cells) compared to HA-LiGluK2 wt (n= 36 and n=46 cells, respectively, from 3 independent cultures,  $P < 0.01$ , Student's t test). Right panel. Quantification of integrated fluorescence and density of dendritic Homer1c-GFP clusters in HA-LiGluK2 and HA-LiGluK2 $\Delta$ 16 expressing neurons. Note that the transfection of LiGluK2 $\Delta$ 16 mutant does not alter either the Homer1c expression or the Homer1c dendritic cluster density.

**(G)** Left panel: Representative averaged traces of light-evoked LiGluK2 $\Delta$ 16 receptor-mediated currents in the absence (left panel) or presence (right panel) of Con-A (0.1mg/ml). Similarly to LiGluK2 wt mediated currents, the LiGluK2 $\Delta$ 16 current onset is followed by

fast and profound desensitization, abolished by the application of Con A. **(H)** Summary of median diffusion coefficient and IQR (left panel) and MSD vs time curve (middle) of extrasynaptic LiGluK2 $\Delta$ 16 in the closed state ( $n_{\text{trajectories}} = 321$ , blue), desensitized state ( $n_{\text{trajectories}} = 276$ , purple) and recovery ( $n_{\text{trajectories}} = 280$ , grey) from 7 neurons,  $P > 0.05$ , Mann–Whitney U-test. **(I)** Representative image of a dendrite portion showing the colocalization (arrows) of N-cadherin (green) with Homer1c (red) in control neurons (upper panel) and in neurons overexpressing the dominant negative mutated N-cadherin (N-cad $\Delta$ E) (lower panel). Note that, in N-cad $\Delta$ E neurons, synaptic N-cadherin is decreased. Scale bar, 1  $\mu$ M. **(J)** Quantification of integrated fluorescence intensity of N-cadherin (left panel) and percentage (right panel) of N-cadherin colocalization with Homer1c in control neurons (wt,  $n=50$  cells) and in neurons overexpressing N-cad $\Delta$ E ( $\Delta$ E,  $n= 40$  cells). **(K)** Representative fluorescence image of the distribution and colocalization of surface HA-LiGluK2 (green) and the postsynaptic marker Homer1c (red) in neurons overexpressing the dominant negative N-cad $\Delta$ E mutant. Scale bar, 5  $\mu$ M. Right panel: Magnification of the portion of dendrite framed on the left panel, showing HA-LiGluK2 clusters (top), Homer1c clusters (middle) and the LiGluK2-Homer1c colocalization (bottom). Arrows indicate synaptic clusters. Scale bar, 1  $\mu$ M. **(L)** Left panel. Summary of immunocytochemistry experiments showing the integrated intensity of HA-LiGluK2 and the HA-LiGluK2 dendritic cluster density in neurons overexpressing N-cad $\Delta$ E with respect to neurons expressing HA-LiGluK2 alone ( $n=51$  cells and  $n=73$  cells, respectively, from 4 independent cultures,  $P < 0.01$ , Student's t test). Please note that the transfection of N-cad $\Delta$ E reduced the expression of HA-LiGluK2 while it left the HA-LiGluK2 dendritic cluster density unchanged. Right panel. Quantification of integrated fluorescence and density of dendritic Homer1c-GFP clusters in neurons overexpressing N-cad $\Delta$ E with respect to neurons expressing HA-LiGluK2 alone. Please note that the N-cad $\Delta$ E overexpression does not alter either the Homer1c expression or the Homer1c dendritic cluster density. **(M)** Left panel: Representative averaged traces of light-evoked LiGluK2 receptor-mediated currents in neurons overexpressing N-cad $\Delta$ E, in the absence (left panel) or presence (right panel) of Con-A (0.1mg/ml). **(N)** Summary of median diffusion coefficient and IQR (left panel) and MSD vs time curve (right panel) of extrasynaptic LiGluK2 receptors in neurons expressing N-cad $\Delta$ E in the closed state ( $n_{\text{trajectories}} = 194$ , blue), desensitized state ( $n_{\text{trajectories}} = 188$ , purple) and closed recovery state ( $n_{\text{trajectories}} = 174$ , grey, from 5 neurons, ns, Mann–Whitney U-test). Unless otherwise stated data are presented as mean  $\pm$  SEM, \* $P < 0.05$ ; \*\* $P < 0.01$ ; \*\*\* $P < 0.005$ ; ns: non-significant.



**Figure S4**

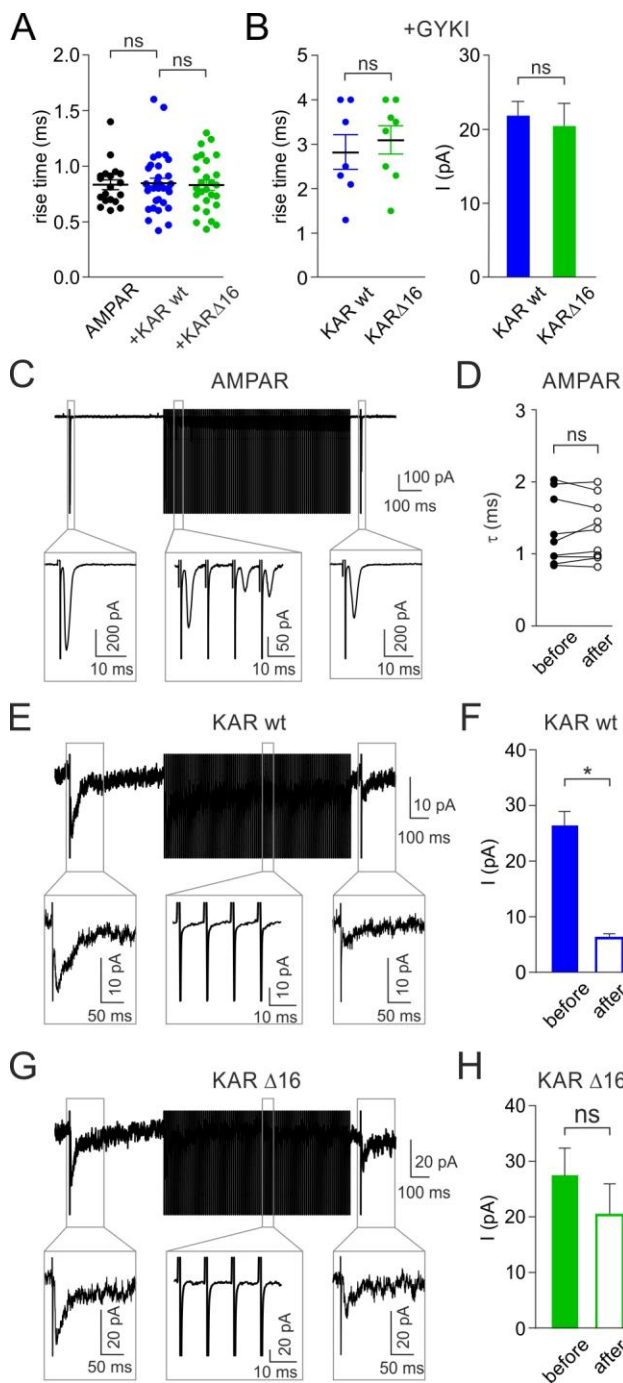


**Figure S4. Electrophysiological properties of eEPSC mediated by AMPA, kainate or mixed AMPA/kainate receptors (Related to Figure 5). (A)** Scatter dot plot of rise time of eEPSC mediated by AMPA receptors (black), AMPA/LiGluK2 receptors (blue) and AMPA/LiGluK2 $\Delta$ 16 receptors (green). **(B)** Left panel: Scatter dot plot of rise time of eEPSC mediated by LiGluK2 (blue) and LiGluK2 $\Delta$ 16 kainate receptors (green). Right panel: Bar graphs of average amplitude of eEPSC mediated by LiGluK2 (blue) and LiGluK2 $\Delta$ 16 kainate receptors (green). **(C)** Top: Representative

“pure” AMPA receptors-mediated eEPSCs recorded in a hippocampal neuron during the delivery of 100 Hz protocol. The protocol, used to monitor changes in the eEPSCs decay kinetics following massive receptor desensitization consisted of: i) delivery of a minimal stimulation to evoke an eEPSCs (before), ii) 500 ms gap, iii) the delivery of a depolarization train for 1 second, iv) 50 ms gap and, v) delivery of a second eEPSCs (after) (see methods). Bottom: magnification of the framed area showing EPSCs mediated by AMPAR before, during and after the train. **(D)** Matched time constants of AMPA receptors-mediated eEPSC before and after the train. **(E)** Top: Representative eEPSCs mediated by LiGluK2 receptors pharmacologically isolated by using GYKI 10  $\mu$ M recorded in a hippocampal neuron during the delivery of 100 Hz protocol. The protocol, used to monitor changes in the eEPSCs decay kinetics following massive receptor desensitization consisted of: i) delivery of a minimal stimulation to evoke an eEPSCs (before), ii) 500 ms gap, iii) the delivery of a depolarization train for 1 second, iv) 50 ms gap and, v) delivery of a second eEPSCs (after) (see methods). Bottom: magnification of the framed area showing EPSCs mediated by KARs before, during and after the 100 Hz train. **(F)** Bar graphs of average amplitude of eEPSC mediated by LiGluK2 kainate receptors before and after the application of the train. Note the profound decrease of the current amplitude after the train. **(G)** Top: Representative eEPSCs mediated by LiGluK2 $\Delta$ 16 receptors pharmacologically isolated by using GYKI 10  $\mu$ M, recorded in a hippocampal neuron during the delivery of 100 Hz protocol. The protocol, used to monitor changes in the eEPSCs decay kinetics following massive receptor desensitization consisted of: i) delivery of a minimal stimulation to evoke an eEPSCs (before), ii) 500 ms gap, iii) the delivery of a depolarization train for 1 second, iv) 50 ms gap and, v) delivery of a second eEPSCs (after) (see methods). Bottom: magnification of the framed area showing EPSCs mediated by LiGluK2 $\Delta$ 16 receptors before, during and after the 100 Hz train. **(H)** Bar graphs of average amplitude of eEPSC mediated by LiGluK2 $\Delta$ 16 kainate receptors before and after the 100 Hz train. Data are presented as mean  $\pm$  SEM, \*P<0.05; ns: non-significant.

**Figure S5**

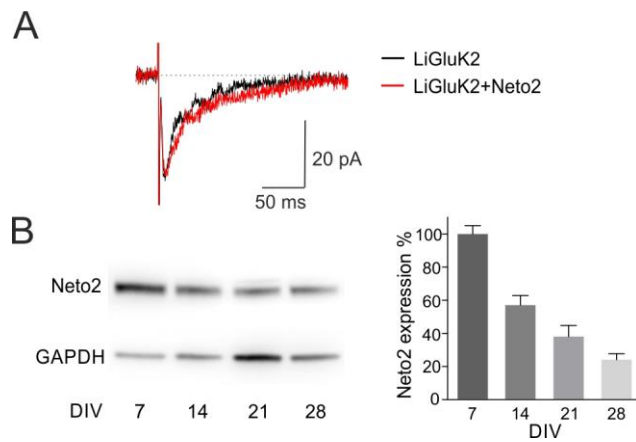


**Figure S5. Neto2 expression in hippocampal cultured neurons (Related to Figure 5)**

**(A)** Example traces of kainate mediated eEPSC in hippocampal neuron overexpressing LiGluK2 alone (black trace) or co-transfected with Neto2 (red trace). Note that the presence of Neto2 does not change the decay kinetics of the kainate current. **(B)** Left panel. Western Blot of Neto2 from cultured neurons at DIV 7, 14, 21 and 28, showing the decrease of the expression of Neto2 over development. Right panel. Quantification of Neto2 at the indicated DIV, normalized to Neto2 level at DIV 7 (n=5). Data are presented as mean  $\pm$  SEM, \*P<0.05; ns: non-significant.

Figure S6

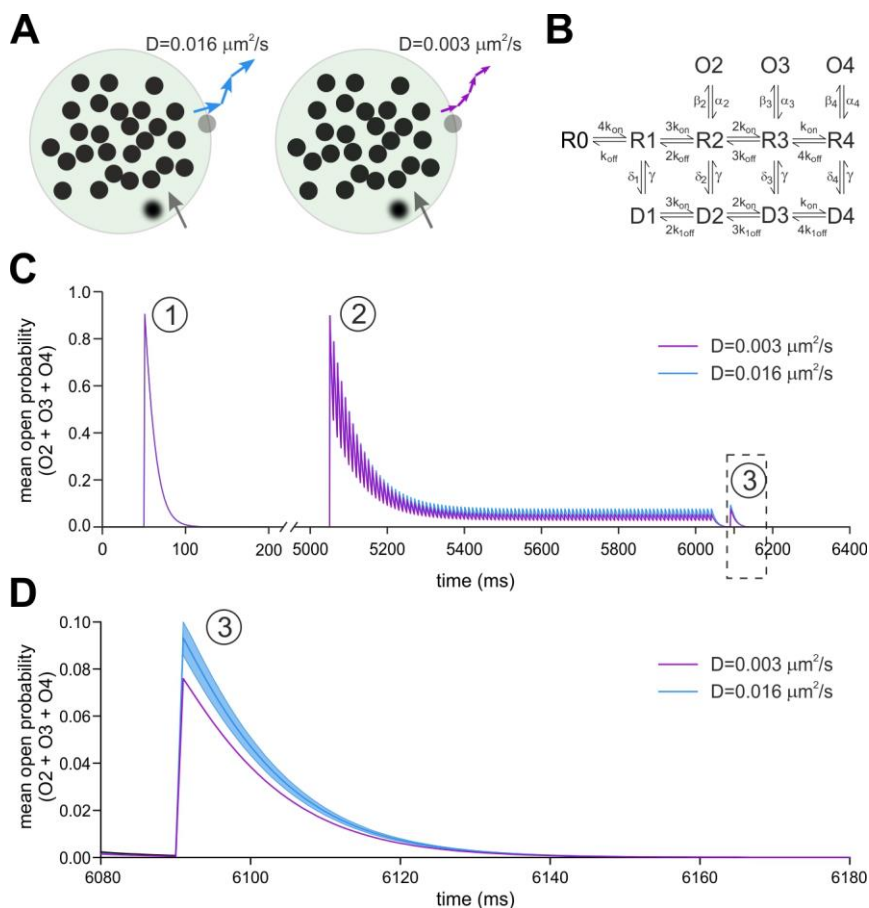


**Figure S6. Modeling of impact of receptor mobility on synaptic KARs-mediated responses (Related to Figure 5).** **A.** Schematic representation of the synaptic disk and kainate receptors that have been used for modeling the synaptic receptor exchange in the conditions of both “high mobility” (i.e., closed receptor,  $D=0.016 \mu\text{m}^2/\text{s}$ , left) and “low mobility” (i.e., open/desensitized receptor,  $D = 0.003 \mu\text{m}^2/\text{s}$ , right). Receptors were uniformly distributed on the synaptic disk (of radius  $0.1 \mu\text{m}$ ) at the density of  $1100 \text{ receptors}/\mu\text{m}^2$  (i.e. 27 receptors). Receptors leaving the synaptic disk (grey dot) with high (blue arrow) and low mobility (purple) are substituted by a naive receptor (blurred dot with grey arrow) in a random position in the disk. “Synaptic” receptors exchanged with the “extra-synaptic” ones with probability  $p = 0.41$ , in the closed naïve state, and  $p = 0.09$ , in the

open/desensitized states. These probabilities were used as weighting factors given to the naive receptors and the complementary weights to the immobile receptors (i.e. ever present/active in the synapse). Such difference in “exchange probability” observed in the “lower receptor mobility” configuration resulted in a significantly higher extent of desensitization (see panel C and D). **B.** Kinetic scheme used to simulate the KAR-mediated EPSCs adapted from Barberis et al., (2008). The rate constants (optimized to achieve the best formal fit of the experimental KAR-EPSCs decay time and desensitization) are (in  $\text{ms}^{-1} \text{mM}^{-1}$ ):  $k_{\text{on}}=15$ ;  $k_{\text{off}}=1.8$ ;  $k_{1\text{off}}=0.9$ ;  $\beta_2=24$ ;  $\beta_3=24$ ;  $\beta_4=24$ ;  $\alpha_2=0.8$ ;  $\alpha_3=0.8$ ;  $\alpha_4=0.8$ ;  $\delta_1=0.125$ ;  $\delta_2=0.25$ ;  $\delta_3=0.5$ ;  $\delta_4=1$ ;  $\gamma=0.0008$ . KARs-mediated EPSCs were elicited by delivering to synaptic receptor a synaptic-like glutamate pulse (0.3 ms, 1mM). **C.** Mean cumulative open probability ( $O_2+O_3+O_4$ ) of the kinetic scheme (in panel B) when synaptic kainate receptors were activated by: i) a control pulse to induce a simulated KAR-mediated EPSC (indicated as ①); ii) a train of KAR-mediated EPSCs (1s @100Hz) to induce massive receptor desensitization (②), and iii) a “test” pulse delivered 50 ms after the train to monitor the degree of receptor desensitization from KARs-EPSC amplitude (③). Such protocol was delivered in conditions of receptor “high mobility” (blue trace) and “low mobility” (purple trace). **D.** Magnification of simulated EPSCs at time point (③) (framed in B) in conditions of receptor “high mobility” (blue traces) and low mobility” (purple trace). Shaded areas indicate SEM. The code needed to reproduce the simulations in Figure S6 is available at github: [thierrynieus/Kainate-receptor-activation-shapes-short-term-synaptic-plasticity-by-controlling-receptor-lateral-mo](https://github.com/thierrynieus/Kainate-receptor-activation-shapes-short-term-synaptic-plasticity-by-controlling-receptor-lateral-mo)